Appendix 7

pages 1 - 11

PROBE CALIBRATION

ETH Eidgenössische Technische Hochschule Zürich
Ecole polytechnique fédérale de Zurich
Politecnico federale di Zurigo
Swiss Federal Institute of Technology Zuri

Prof. Dr. Niels Kuster

Tel: +41 1 632 2737, Fax: +41 1 632 10

Institut für Feldtheorie
und Höchstfrequenztechnik
ETH Zürich
CH-8092 Zürich

Mr. Illkka Pankinaho
Nokia Mobile Phones
NMP/R&D
P.O. Box 86
FIN-24101 Salo
Finland

Zurich, 2 December 1995

Mobile Phone Certification

Dear Mr. ~~Pankinaho,~~ ILKKA

In mid-September, we promised to send preprints of the paper which describes the calibration procedure we developed during the last months. We would appreciate any suggestions and comments, since a thorough calibration is fundamental to enforce the safety limits. In addition, we would like to take this opportunity to inform you about the newest developments towards finalizing the scientific and technical conditions for a type approval.

Uncertainties of Measurements: In connection with the calibration, we peformed an analysis which assessed the total uncertainty of SAR measurements in shell phantoms. The results are promising. The total uncertainty can be kept below ±20% at 900 MHz. A project to further reduce these uncertainties and to develop a standard calibration procedure has now been submitted to the EU program "Standards, Measurements & Testing."

Phantom: Another open issue is the verification that the absorption in homogeneous human phantoms represents well the actual spatial peak absorption in the user. In one study, in close cooperation with the research center of German Telekom, absorption induced in three numerical and three experimental phantoms were compared for the mobile communications frequency at 900 MHz. The various phantoms and our findings are briefly described in the attachment.

Requirements of a Certification Procedure: In connection with the recent WTR workshop in Rome, we defined the scientific pre-condition necessary to implement a certification procedure. The manuscript also reflects the requirements which were discussed within CENELEC's TC111 Working group on Mobile Telecommunications Equipment. Please find the manuscript in the attachment as well.

DASY: Schmid & Partner Engineering AG (SPEAG) has started the development of DASY3. Besides a general revision and extension of the DASY2 hardware and software, the main objectives of DASY3 are improved spatial resolution, improved precision and improved time efficiency. DASY3 will be largely compatible with DASY2, although some of the new functions will not be fully usable without minor hardware updates. SPEAG will keep you informed with respect to these developments.

The temperature probes which have been developed for the previously mentioned calibration study will soon be commercially available. The prototype showed a sensitivity of about <0.1 mK/s. It might be interesting to all DASY users that this probe will be fully compatible with DASY2, DASY3 and DASYmini. The active volume of about 1 mm3 is ideal for those laboratories which plan to do calibration or SAR measurements in very small structures.

Part of the industry was interested in a video of DASY2 to demonstrate the test procedure to their customers . Since we already had a video for other occasions, we adapted it to these requests and now have copies available. If you are interested, please return the enclosed form by mail or fax. If you want copies of any of the publications listed on that form, we would be happy to send you these copies as well.

If you have any questions regarding our activities in the area of mobile phone certification, please do not hesitate to contact me. For questions regarding the dosimetric assessment system DASY, I suggest you contact SPEAG directly (phone: +41 52 232 7272, FAX: +41 52 232 7127).

Yours sincerely

Prof. Dr. N. Kuster

Encl.

Broadband Calibration of E-Field Probes in Lossy Media

Klaus Meier, Michael Burkhardt, Thomas Schmid and Niels Kuster

Abstract— **A broadband calibration procedure for E-field probes that minimizes the overall uncertainties inherent in E-field measurements in lossy dielectric liquids has been developed. The analysis of the calibration requirements shows that probes that are symmetrical with respect to their axis greatly facilitate accurate calibration, since the calibration procedure can be divided into several discrete steps. Such a procedure is presented and analyzed with respect to its uncertainties. Absolute calibration is performed at three frequencies (450 MHz, 900 MHz and 1.8 GHz) and in different tissue-simulating liquids. The parameters obtained are verified by numerical simulations of the probe in the surrounding media. Such simulations allow the assessment of some of the calibration parameters with sufficient accuracy in cases where the experimental determination would be too tedious and time-consuming.**

I. Introduction

The interaction of high-frequency electromagnetic fields with biological matter has been the object of growing interest for several years. Miniature E-field probes have been developed to determine experimentally the induced electric field in actual tissue or tissue-simulating liquids.

In view of the phenomenal growth of the mobile communications market, the telecommunications industry has lately recognized the need to test its mobile telephones for compliance with today's safety limits. The key value for dosimetric assessments in general and compliance tests in particular is the maximum tolerable absorbed power per tissue mass in mW/g, known as the specific absorption rate (SAR). The local SAR can be determined experimentally by measuring either the induced electrical field strength or the temperature rise in tissue.

$$SAR = \frac{\sigma}{\rho}E^2 = c\frac{\partial T}{\partial t} \qquad (1)$$

where σ is the conductivity, ρ is the mass density and c is the specific heat of the tissue at the site of measurement.

Since measurements using thermal probes do not provide an adequate degree of efficiency and sensitivity for compliance-testing of consumer products, the research up until today has been focused on small isotropic E-field probes.

The original design of a miniaturized isotropic E-field probe for use in tissue-simulating liquids goes back to Bassen *et al.* [1] Recently the authors presented a new probe design [2] with significantly improved performance.

In view of the significance of, and the difficulties involved in, accurate calibration, surprisingly little has been published so far about broadband calibration of isotropic E-field probes in dielectric materials. In [3] a calibration procedure in an S-band waveguide at a single frequency of 2.45 GHz is described. However, the calibration uncertainties due to the dependence of the probe sensitivity on polarization, frequency, dielectric parameters of the surrounding media and spatial resolution have only been marginally addressed. In this paper these issues are analyzed and a calibration procedure enabling accurate calibration of the probes for a broad frequency range in two lossy dielectric liquids is described. A flexible setup has been chosen in order to study ways of minimizing the uncertainty of dosimetric assessments in the frequency range of mobile communications.

Submitted to IEEE Transactions on Microwave Technique and Technology - October 1995.

The authors are with the Swiss Federal Institute of Technology (ETH), CH-8092 Zurich, Switzerland.

II. E-Field Probe Design and Measurement Errors

The main requirements for E-field probes in any type of surrounding medium are:

- high degree of isotropy in various media;
- high sensitivity and linear response over a broad frequency range;
- high spatial resolution (small tip size); and
- low interaction with the measured field.

E-field probes with isotropic response can be achieved by the orthogonal positioning of three sensors that are sensitive to one E-field component each. Short dipoles or small E-field-sensitive crystals have these characteristics. In miniaturized E-field probes small dipoles with diode rectifiers are mainly used, because they offer the greatest sensitivity and have a linear response over a wide frequency range. A design with a triangular core was chosen for the new E-field probe. This design provides a small outline and shows a high degree of symmetry (Figure 1). The sensors themselves consist of three small dipoles (3 mm in length) directly loaded with a Schottky diode and connected via resistive lines to the data acquisition electronics.

In the following, a number of design problems of these probe types are mentioned; some of them apply to other probe types as well. A more detailed description of the probes is given in [2].

1.) *Secondary modes of reception:* Resistive lines are used to transmit the signal from the rectifier diodes to the evaluation electronics. The interaction of these lines with the field should be minimal. Nevertheless, RF signals can be picked up by the lines and detected and rectified by the diodes. These secondary reception modes appear mainly at lower frequencies, where the impedance of the dipole and the diodes is very high and can produce disturbed directivity characteristics. Special filtering techniques or high

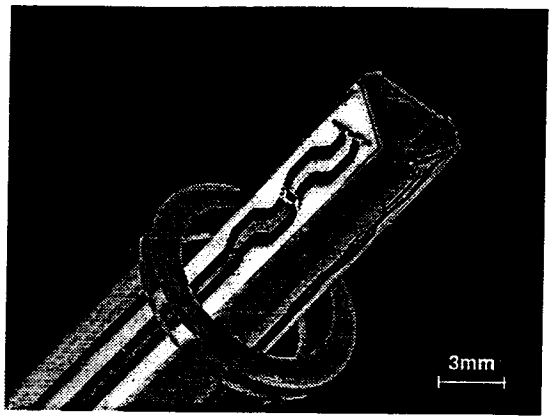

Fig. 1. Tip of the E-field probe. The tip encapsulation has been removed. One 3 mm long dipole and the diode can be seen. In the center of the core is the opening for a built-in optical proximity sensor.

ohmic lines can reduce this effect. [2]

2.) *Influence of the probe materials on the field:* Any dielectric material around electric dipoles can have an effect on the local signal strength inside the probe. It is obvious from the construction of these probes that the influence on E-field components normal to the probe axis will be different from that on E-field component parallel to the probe axis. Furthermore, this difference in sensitivity depends on the surrounding medium. This results in poor isotropy in planes along the probe axis. In [2], several methods are presented to compensate for these effects. In any case the directivity characteristic of the probe will be different in different media. This has to be taken into account when calibrating the probe in a specific medium.

3.) *Influence of the probe on nonhomogeneous fields:* The disturbance caused by the probe on nonhomogeneous fields depends both on the geometrical and material properties of the probe and on the nature of the field itself. The influence of these effects must be investigated in each case. Errors in SAR readings can occur when using the probe in the immediate vicinity of material discontinuities – for instance, when the probe approaches the surface of a shell phantom (see also Figures 6 to 9). By performing measurements at different distances from the surface and extrapolating to the surface, corrected SAR values for the vicinity of the surface can be obtained.

4.) *Spatial resolution:* Another source of error in nonhomogeneous fields arises from the spacing between the dipole centers in the probe. Since each field component is measured at a slightly different location, discrepancies are to be expected when the field's magnitude or direction varies greatly within the probe's dimensions. By turning the probe along its long axis, the measurement locations of the three sensors shift and a further isotropy error will occur.

Therefore, a calibration setup that minimizes these errors must be carefully chosen.

III. Calibration Requirements

The three output signals from an isotropic E-field probe with three orthogonally positioned sensors must be evaluated to give a reading that corresponds to the SAR at the measurement site *in the absence of the probe.* The relation between the field and the sensor signals depends on various factors:

- design and construction materials of the probe;
- electrical properties of the surrounding media;
- direction and polarization of the field;
- field gradient at the measurement site;
- RF characteristics of the antenna, the rectifying element and the transmission line;
- higher order modes or different reception modes in the probe;
- sensitivity of the rectifier; and
- characteristics of the evaluation circuit for the rectified signals.

Each calibration essentially attempts to describe these effects quantitatively, so that correct SAR values can be obtained under various measurement conditions. Furthermore, it is important to know the absolute uncertainty and the validity range of the calibration. To keep the number of calibration parameters and calibration measurements low, it is crucial to separate the above-listed influences and quantify them individually. An effective way must be found to reduce the effect of any possible further errors that can arise under various measurement conditions. The probe design is a deciding factor in this regard. For our dosimetric probes, a three-step calibration process has proven to be the most effective approach:

$$|E^2| = \sum_{i=1}^{3} \frac{f_i(V_i)}{\eta_i \gamma_i} \tag{2}$$

a) $f_i(V_i)$: The rectified signal of each sensor (V_i) is linearized. The linearization function depends on the characteristics of the rectifier and the evaluation circuit. It can be described as a function of the magnitude of the rectified signal and can be assessed easily by a power sweep of the exciting field. When the rectifying elements and evaluation channels are identical, the same function f ($f_i(V_i) = f(V_i)$) can be used for all sensors. In the case of amplitude-modulated signals, the timing characteristics of the evaluation circuit must also be taken into account, unless the signal stays within the "square law" region of the detector element, or the evaluation is rapid enough to keep pace with the modulation. For pulsed signals with a known crest factor, a simple correction formula can be given; for arbitrary modulations, however, a more sophisticated signal analysis is necessary.

b) η_i: These factors describe the absolute sensitivities of the probe sensors (μV/(V/m)^2) in air for which γ_i is equal to one. They depend on the probe construction materials, the sensor positioning and the RF characteristics of the sensor components. If detector diodes are used as rectifying elements, the parasitic capacitance, which is generally not precisely specified, influences the RF behavior.

Therefore, the factors η_i will be different for each sensor, even if the sensors are positioned in a symmetrical fashion. These factors can be assessed by standard probe calibration procedures (see Section IV). All error sources (isotropy, frequency linearity) must be investigated during this calibration in order to assess the calibration factors for an average measurement situation and to evaluate the error and validity range of the calibration. For broadband E-field probes, the calibration factors are independent of the frequency over a wide range (2 to 3 decades) and can thus be considered to be constants.

c) γ_i: These factors describe the ratio of the sensitivity of the probe sensors in different media to their sensitivity in air. These usually depend both on the surrounding material and the frequency and on the constructional materials and the design of the probe. They will be identical for each probe of the same type. In the case of symmetrical sensor positioning they will even be identical for each sensor ($\gamma_i = \gamma$). This implies that the (time-consuming) assessment of these calibration factors (see Sections V and VI) need to be done only once for each probe type, and not for each individual probe. γ will hereafter be called the "conversion factor".

The separation of the calibration factor in a probe and sensor dependent factor η_i and a probe type and situation-dependent conversion factor γ_i is an approximation that is based on various assumptions:

- The variation of the dipole impedance caused by the surrounding medium is the same for all sensors.
- The local E-field distribution in the area of the sensors inside the probe only depends in magnitude on the surrounding medium. In symmetrical probes this condition can be regarded more leniently.
- The constructional differences (manufacturing tolerances) between probes of the same type are small.

The validity of these assumptions depends largely on the probe's design. Measurements and simulations of our probes have established the feasibility of this calibration procedure. However, it is necessary to reassess the deviation from isotropy in liquid, since it may differ from air. (see Section II).

At higher frequencies and in lossy media, the fields have high gradients. If the gradient is significant within the probe's dimensions, a calibration reference point in the probe must be defined. The field gradient will result in further isotropy errors depending on the probe's alignment with respect to the direction of the field gradient. For the best calibration results, the calibration setup should be as close as possible to the actual measuring situation.

IV. Calibration in Air

To calibrate the probe in air, a well-defined measurement volume with an absolutely known and largely homogeneous electrical field is necessary. The field strength can be measured with a standard calibrated probe, if available; otherwise, it must be determined from power measurements. Several methods are used to produce such fields:

a) Far field of standard radiators: These calibrations are done in free space or in anechoic chambers. The open measurement area permits the positioning of the probe easily at any angle towards the field. The radiated power can be measured with high accuracy. Errors in the determination of the antenna gain and reflections limit the absolute accuracy of this calibration method to approximately ± 0.5 dB.

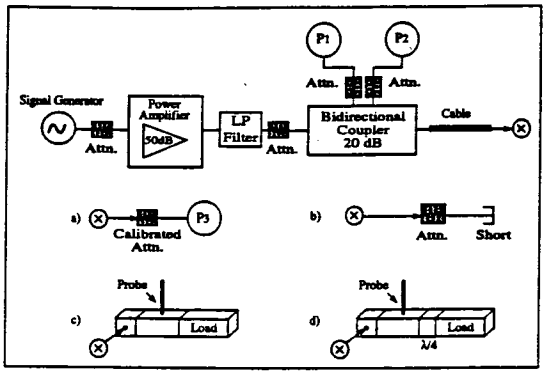

Fig. 2. Setup for calibration in waveguides (air). Measurements *a* and *b* to calibrate the power meters P_1 and P_2. P_3 is a high-precision meter. Probe measurements *c* and *d* with different distances to load.

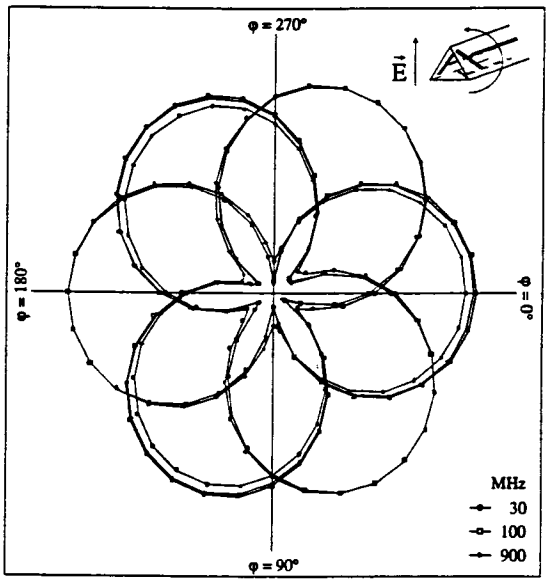

Fig. 3. Receiving pattern of the three orthogonally arranged dipoles after calibration in air. E-field is normal to the probe axis.

b) Near field of radiators: In the near field, it is not easy to determine the absolute field strength. However, the direction of the field vector is often determined by simple symmetry considerations. These fields can be used to measure the relative directivity of the probe when the field gradient is small compared to the probe dimensions.

c) TEM cells produce a homogeneous TEM wave in a limited volume ($\ll$ wavelength). The highest usable frequency is determined by the existence of higher-order propagation modes (200 MHz to 1.5 GHz, depending on the cell size). The power can be measured at the output of the cell. The accuracy is limited by cell impedance variations due to constructional inaccuracies. The discontinuities in the construction (edges, access openings) produce field deviations

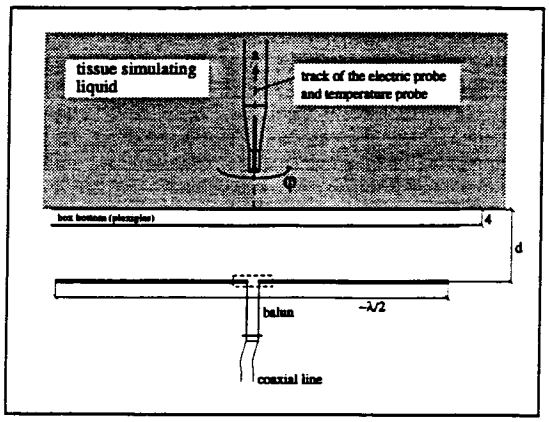

Fig. 4. Experimental setup. On the top is the Plexiglas box filled with the simulating liquid. At the bottom is the dipole. The temperature probes and the E-field probe are positioned directly above the dipole feedpoint.

from the theoretical TEM mode. An absolute accuracy of ± 0.4 dB is possible.

d) GTEM cells have no discontinuities and can be used from DC to several GHz. The calibration volume can have dimensions of several wavelengths. The reflections from the built-in absorber and load produce standing waves, which limit the absolute accuracy of GTEM cells to ± 1 to ± 3 dB.

e) Waveguides produce well-defined fields in small volumes and a limited frequency band. With high-precision components (loads, lines, adaptors to coaxial lines) and error compensation, the field can be determined to be within $\pm 2\%$. However, the influence of the probe itself on the field must be carefully investigated.

For the absolute probe calibration in air, we used methods c) and e). At frequencies over 1 GHz we measured in standard waveguides R22 and R26, with a setup according to Figure 2. The probe is rotated around its axis with a positioning accuracy at the probe tip of better than ± 0.1 mm. Absolute accuracy of the calibration is given for an average in the directivity and lies within $\pm 5\%$ (The linearity over different frequencies and waveguides is better than $\pm 2\%$.). At frequencies below 1 GHz, a TEM cell ifi110 was used for calibration (Figure 3).

The agreement in absolute value with the measurements in the waveguides is better than could be expected from the cell data (within $\pm 3\%$). Waveguide measurements at 900 MHz will be performed to confirm this agreement. As the directivity for all rotational angles of the probe cannot be determined in waveguides, a near-field exposure situation was used. For higher frequencies, the center point over an open waveguide was chosen as the measurement site and, for lower frequencies, the field in the symmetry plane of highly symmetrical standard dipoles.

V. Calibration in Lossy Dielectric Liquids

A. Setup

To determine the conversion factor γ, a well-defined SAR distribution inside the dielectric material for which the probe must be calibrated is needed. Setups are preferred which allow the computation of the field inside the dielectric material analytically or by numerical simulations. One way would be a dielectric slab in a rectangular waveguide. Although the induced fields are well defined and can be determined easily if the emergence of spurious higher modes can be sufficiently suppressed, the setup is very narrow-banded.

Another setup used in [4] is the simulation of a dielectric half-space, which is exposed to a $\lambda/2$ dipole parallel aligned to the surface of this half-space (Figure 4). This configuration can be accurately simulated by using numerical techniques, since the SAR on the axis is predominantly proportional to the square of the antenna feedpoint current and not to the output power. However, experimentally, the feedpoint current can be assessed only with fairly large uncertainties of no better than $\pm 10\%$.

Nevertheless this setup was chosen because:

- It is easy to build up and to handle.
- It provides much greater flexibility since a broad frequency range can be covered by the same setup.
- It is a good representation of the test situation implemented for dosimetric assessments of mobile communications devices [5].
- In lossy dielectric liquids, the local SAR values can be experimentally measured by small thermal probes according to equation (1) at high power levels.

The half-space is simulated by an acrylic glass box ($600 \times 300 \times 200\,\text{mm}^3$) filled with the lossy dielectric liquid. The thickness of the acrylic glass box phantom is 4 mm. The dipoles are placed parallel to the dielectric surface at distances that are small compared to the dimensions of the box and to the distance from the floor. The floor is lined with absorbers.

The dipole used at 450 MHz is a Stoddard dipole 310 mm long, and at 900 MHz a high-precision dipole 147 mm long and 3.6 mm in diameter is used. In both cases, the dipoles are driven by an HP8656B generator and a broadband RF power amplifier (Kalmus Model 717C, 100 W output power). A bidirectional coupler HP775D monitors the forward and reflected power. The 1.8 GHz dipole is 73.5 mm in length and has a diameter of 2.25 mm. Losses along the coupler and the lines are taken into account.

In the following, the conversion factors γ for brain-simulating tissues at 450 MHz, 900 MHz and 1800 MHz are determined.

B. Brain Simulating Liquids

The simulating liquids for brain tissue at 450 MHz and 900 MHz consist of sugar, water, NaCl and Hydroxyethylcellulosis (HEC). [6] For brain tissue at 1.8 GHz, two different liquids were used. The first was based on a simple sugar-water solution without any salt (free ions). Nevertheless, the conductivity of such a solution was still higher than most recent data for living tissue [7] would suggest (Table I). At frequencies higher than 1 GHz, the bound sugar-water complexes begin to determine the conductivity level of the liquid. Therefore, in a second approach, sugar was replaced by butyldigol (2-(2-butoxyethoxy)ethanolbutyl),

TABLE I

DIELECTRIC PROPERTIES OF BRAIN TISSUE-SIMULATING LIQUIDS AT THE TESTED FREQUENCIES. AT 1.8 GHz, TWO LIQUIDS WERE USED: SUGAR-WATER SOLUTION (A) AND BUTYLDIGOL-WATER SOLUTION (B).

Frequency [MHz]	ϵ_r		σ [mho/m]	
450	47.0	±5%	0.43	±6%
900	40.0	±5%	0.87	±6%
1800A	40.5	±5%	1.75	±6%
1800B	41.5	±5%	1.25	±6%

which, when dissolved in water, shows smaller conductivity values. At the same ϵ_r value, the conductivity could be reduced from 1.75 to 1.25 mho/m. The electrical parameters were measured by an open coaxial method using the HP 85070A Dielectric Probe Kit. To verify the open coaxial method, we determined the electrical parameters using the slotted-line method. The agreement was within 4%. Table I gives an overview. The temperature dependence of the liquid's parameter was also checked. In the temperature range between 15° C and 30° C, a change of 5% was measured, which lies within the uncertainty of the permittivity measurement method.

The specific thermal constant c was determined using a simple calorimetric procedure with an accuracy of better than ±4%. The specific density ρ and c depend mainly on the ratio between sugar and water. For brain tissue-simulating liquids, c was determined to be 2.85 J/K/g ±4% with a specific density (ρ) of 1.30 g/cm^3 ±1%. Comparison of these values for c with data from literature shows considerable agreement. Gucker *et al.* measured 2.90 J/K/g for a similar aqueous sucrose solution. [8] The value for the brain tissue-simulating liquid which uses the sugar substitute Buthyldigol is 3.58 J/K/g (ρ = 0.98 g/cm^3 ±1%).

C. Temperature Probe

The measurement of the local SAR by temperature probes has the advantage that temperature is a scalar value. Small sensors can therefore be easily produced. Immunity of the temperature probes towards the HF fields must be guaranteed and can be achieved by optical probes or thermistor probes with high resistive lines. [9] The limited temperature sensitivity of theses sensors can be overcome by applying high power.

In this study, the nonmetallic temperature measurement system (SPEAG DASY2) was used to measure the temperature increase. The probe is based on an NTC temperature sensor connected to four resistive lines. [10] The noise level of this system is about 100 times less than that of the two comparable optical devices on the market (±0.001° C averaged over 0.1 s). The noise level for temperature rise measurement over a period of 10 s was found to be better than ±0.1 mK/s. At these high frequencies (450 MHz - 1.8 GHz) the absorption is very local – i.e., close to the feedpoint of the dipole and rapidly decreasing the further it penetrates the tissue. This causes strong temperature gradients inside the liquid. Thus, thermodynamic dissipation processes, such as convection, had to be monitored. The RF power was usually on for about 14 seconds. The corresponding linear temperature increase was evaluated by least-square. After every exposure period, the liquid was stirred until a thermodynamic equilibrium state was reached again before the RF power could be switched on again. The temperature increase in the liquid due to exposure to a 900 MHz field at two distances from the body is shown in Figure 5. The effects of convection were assessed by evaluating different time intervals and were found to be negligible within the first 10 s for sugar-water solution. The solution based on Buthyldigol had considerably lower viscosity, so that the evaluation time had to be reduced to 5 s.

A robot positioned the temperature probe in the liquid by moving it from the top, like the E-field probes, towards the bottom of the box. The disturbance of the probe holder has proven to be negligible.

TABLE II

CONVERSION FACTOR γ, WHICH DESCRIBES THE INCREASE OF SENSITIVITY IN BRAIN TISSUE-SIMULATING LIQUIDS AT THE TESTED FREQUENCIES.

Frequency [MHz]	ϵ_r	σ [mho/m]	γ	
450	47.0	0.43	6.7	±10%
900	40.0	0.87	6.0	±10%
1800A	40.5	1.65	4.8	±10%
1800A	41.0	1.25	4.8	±10%

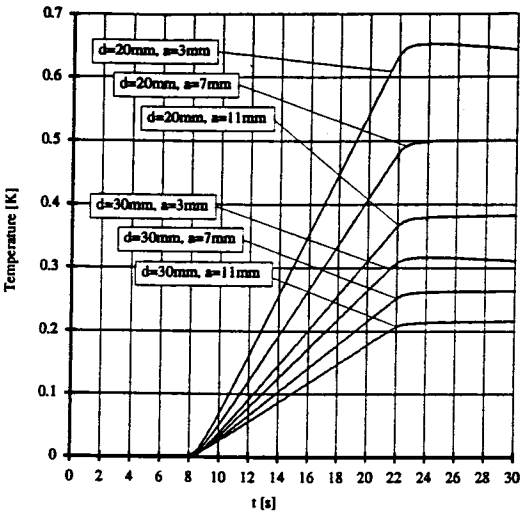

Fig. 5. Temperature increase measured during RF exposure to a 900 MHz field. The power input was 43 dBm. d = dipole distance from the simulating liquid; a = sensor distance from the acrylic glass bottom.

D. Results

The conversion factor γ was determined by comparing the SAR values measured by the temperature probe and by the E-field probe. The measurement points were located on a line normal to the Plexiglas bottom above the dipole

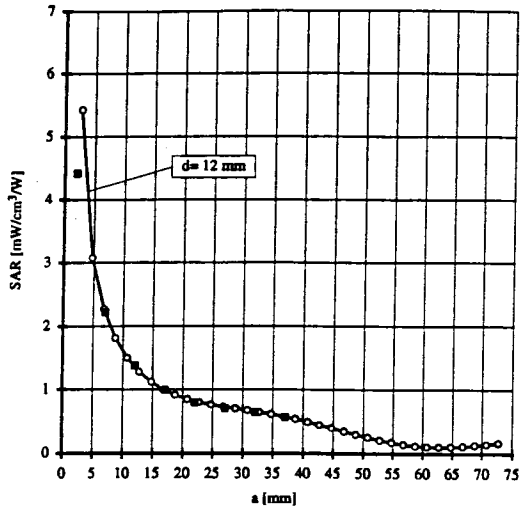

Fig. 6. SAR assessed by E-field (small empty symbols) and temperature measurement (big full symbols) at 450 MHz in brain-simulating liquid (ϵ_r = 47.0 and σ=0.43 mho/m). The SAR was normalized on 1 Watt input power. The frequency was set to 450 MHz. The dipole distance from the body was 12 mm. The conversion factor γ was determined to 6.7 ±10%.

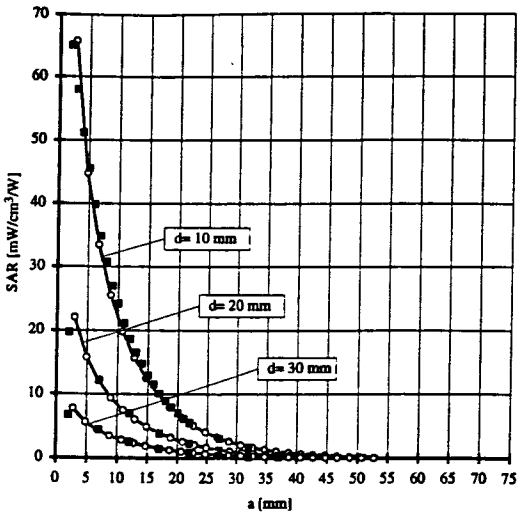

Fig. 8. SAR assessed by E-field (small empty symbols) and temperature measurement (big full symbols) at 1.8 GHz in brain-simulating liquid (ϵ_r = 40.5 and σ=1.75 mho/m). The SAR was normalized on 1 Watt input power. The dipole distances from the body were 10 mm, 20 mm and 30 mm. The conversion factor γ was determined to 4.8 ±10%.

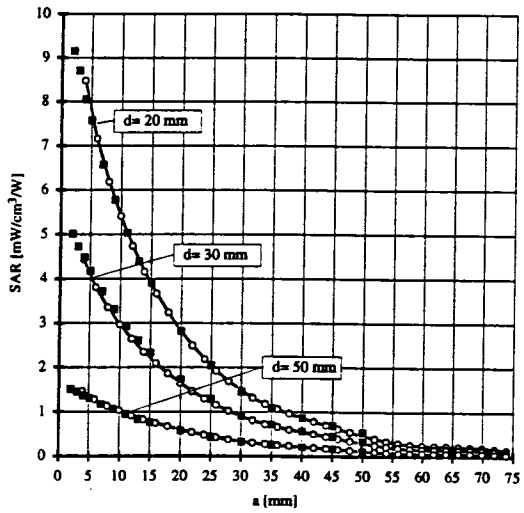

Fig. 7. SAR assessed by E-field (small empty symbols) and temperature measurement (big full symbols) at 900 MHz in brain-simulating liquid (ϵ_r = 40.0 and σ=0.87 mho/m). The SAR was normalized on 1 Watt input power. The dipole distances from the body were 20 mm, 30 mm and 50 mm. The conversion factor γ was determined to 6.0 ±10%.

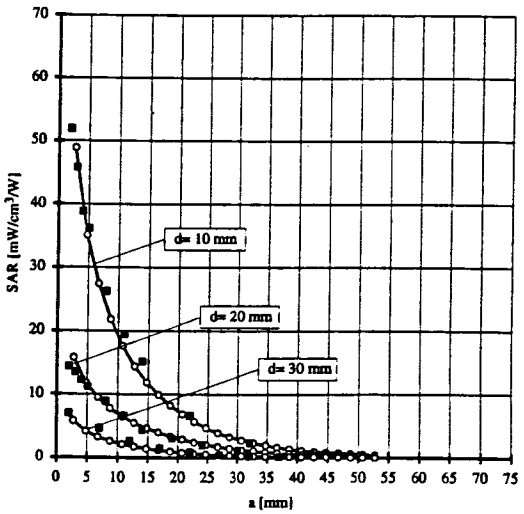

Fig. 9. SAR assessed by E-field (small empty symbols) and temperature measurement (big full symbols) at 1.8 GHz in brain-simulating liquid (ϵ_r = 41.0 and σ=1.25 mho/m). The SAR was normalized on 1 Watt input power. The dipole distances from the body were 10 mm, 20 mm and 30 mm. The conversion factor γ was determined to 4.8 ±10%.

feedpoint (Figure 4). These measurements were repeated at different power levels, at different distances of the RF source from the body and at different frequencies (Figures 6 to 9). The conversion factor was assessed by a least-square procedure considering all measured values. The results for the various tissues are summarized in Table II.

The accuracy of the conversion factor γ is mainly determined by the uncertainties in determining the correct electromagnetic and thermal properties of the tissue-simulating liquid. Using the "slot line" and "open coaxial" methods to determine the conductivity of the liquid introduces an uncertainty of about ±6%. The specific heat of the liquid can be assessed to an accuracy of about ±4%. The E-field probe yields another ±3%. Adding the uncertainty of the positioning of the E-field probe (±1%), of the temperature probe (±2%), and of the power meters (±1%) leads to a total uncertainty of less than ±10%.

VI. Numerical Studies

Three objectives led us to use numerical techniques to simulate the probe embedded in lossy dielectric materials: 1) to study methods to improve the isotropy of the probes [2]; 2) to assess the spatial resolution; and 3) to determine the conversion factor γ computationally, since numerical

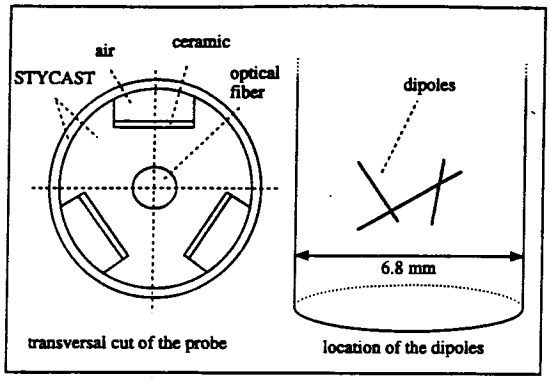

Fig. 10. Computer simulation model: transversal cut of the probe and location of the dipoles.

techniques are less tedious than the experimental approach.

To obtain a deeper insight into the behavior of the conversion factor, two numerical program packages based on two different techniques were used. This had the advantage of the possible cross-validation of the results obtained by both techniques, each of which has its strengths in different areas.

The first one is the 3D MMP software package developed at the Swiss Federal Institute of Technology (ETH). It is a frequency domain boundary technique suited for 2D and 3D scattering problems within piecewise linear, homogeneous and isotropic domains. Details are given in [11] and [12]. The second software package, "MAFIA", was developed at the Technische Hochschule Darmstadt (THD), Germany. The method used is based on the finite integration technique (FIT) and is very similar to an FDTD approach. Details are given in [13] and [14].

A. Modeling of the probe

To study the field distribution inside the probe depending on the electrical parameters of the surrounding media, different discretizations of the E-field probe were chosen. A transversal cut of the probe and a perspectival view with the location of the dipoles inside the probe is shown in Figure 10. Different discretizations with increasing complexity have been compared:

a) The simplest numerical representation of the probe is a simple homogeneous, lossless cylinder 6.8 mm in diameter with a relative permittivity of 2.54. This corresponds to the electrical properties of the microwave material utilized (STYCAST 0005) to build the core of the probe. The length of the cylinder is 15 mm, which has proven to be long enough to study the fields induced in the probe tip. MMP could only be used for this simple homogeneous model of the probe. In MMP, the modeling required about 550 matching points at the boundary of the two domains and 9 multipole expansions. As expected, the maximum errors (<10%) appeared on the matching points at the corners of the probe. In order to minimize these errors and to use a minimal number of expansion functions, the edge of the probe was slightly rounded. About 90,000 voxels were needed to model the whole computational domain within MAFIA, about 5,000 of which were needed for the probe itself. Problems occur at the outer boundaries when using open-boundary conditions and assuming the whole computational domain to be of a lossy material, as in the case of biological tissue. Nevertheless, in choosing a long computational domain in the direction of the wave propagation vector and in considering that the attenuation over one wavelength is very slight, the influence of possible reflected waves was assumed to be less than 3%.

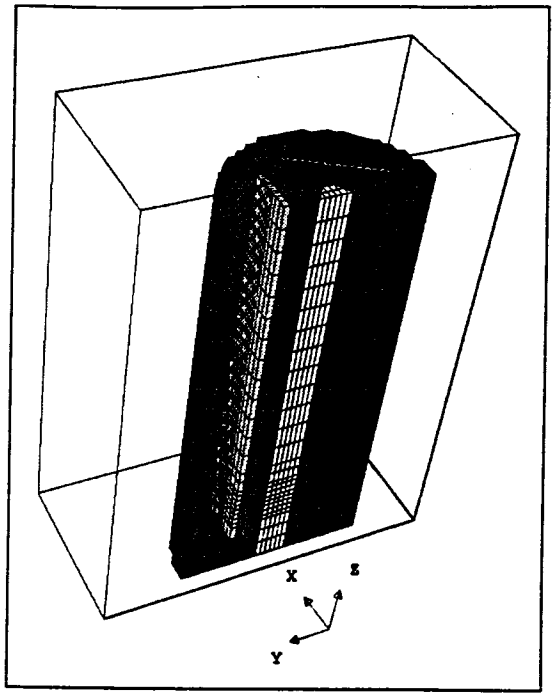

Fig. 11. Computer simulation model: complex model of the probe for the MAFIA simulation tool.

b) A more complex model simulated the optical fiber in the center of the core. The fiber was discretized as a smaller homogeneous cylinder 1 mm in diameter with a relative permittivity of 5 in the center of the STYCAST cylinder.

c) Additional details were incorporated in a further model by the modeling of the three air holes (Figure 10).

d) In the most complex model, three ceramic sheets on which the dipoles and lines are printed were simulated as well (Figure 11). This leads to a discretization with 210,000 voxels, about 37,000 of which were needed for the probe itself.

In all the models the dipoles were not simulated. The conversion factor can be calculated by integrating the electric field at the location of the dipoles, firstly with biological tissue surrounding the structure and then with air around it:

$$\gamma = \frac{\sum_{i=1}^{3} \left(\int_{Dipole_i} \vec{E}\vec{ds}(in\ tissue) \right)^2}{\sum_{i=1}^{3} \left(\int_{Dipole_i} \vec{E}\vec{ds}(in\ air) \right)^2} \qquad (3)$$

As the reference value, the E-field at the location of the dipole center in the absence of the probes was chosen.

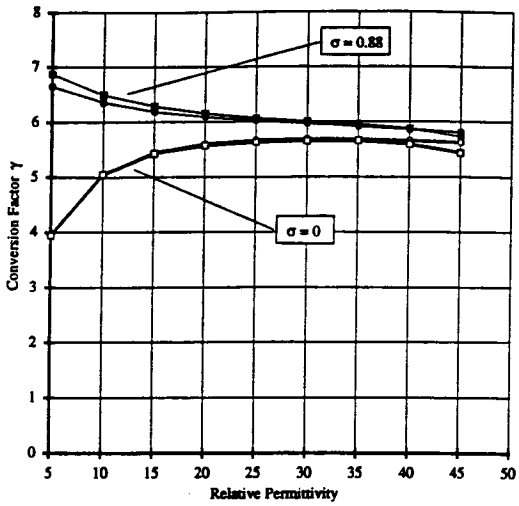

Fig. 12. Simulation: conversion factor at 900 MHz as a function of the relative permittivity of the biological tissue. Done for absorbing biological tissue and nonabsorbing tissue. MAFIA modeling are displayed by squares, MMP modeling by circles.

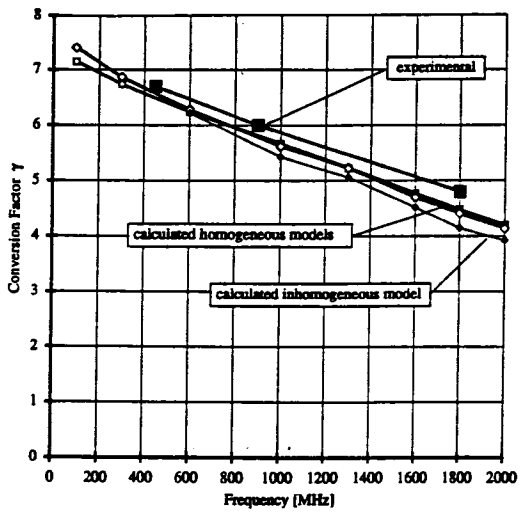

Fig. 14. Experimentally assessed conversion factor for brain tissue-simulating liquid in comparison with the values obtained from numerical simulation for homogeneous (empty symbols) and non-homogeneous (filled symbols) modelings of the probe.

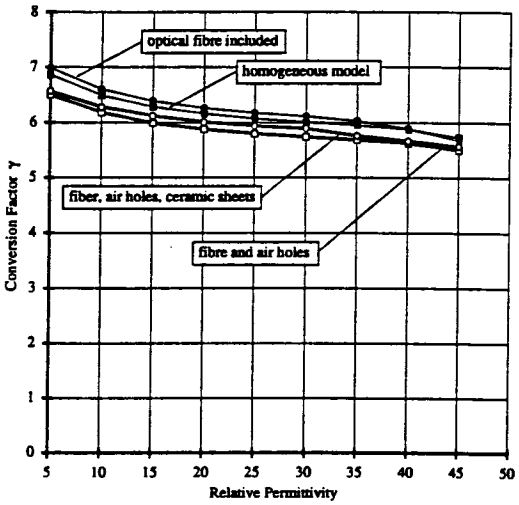

Fig. 13. Simulation: conversion factor as a function of the relative permittivity of the biological tissue for different MAFIA models. The conductivity is 0.88 mho/m, the frequency 900 MHz.

B. Results of the Simulations

The simulations with the simple homogeneous models were performed for different dielectric properties of the probe's surrounding medium. Figure 12 shows the dependence of the probe's conversion factor as a function of the relative permittivity. The frequency of the excitation was set to 900 MHz. These calculations were made for absorbing biological tissue and for nonabsorbing tissue.

The conductivity of the lossy material corresponds to the value used for the experimental investigations (0.88 mho/m, see below). The influence of the conductivity of the lossy material becomes less important for a larger real part of the complex permittivity. Within a wide range of relative permittivities (of biological tissue), the conversion factor or, in other words, the sensitivity of the probe changes by less than 10%. This is even true when changing the conductivity of the biological tissue within a certain range. However, for small real parts of the complex permittivity, the influence of the conductivity on the conversion factor is strong. A comparison of the results of the two methods (MMP and MAFIA) reveals that the difference is less than 1% for the nonabsorbing material and between 1% and 3% for the absorbing material.

In Figure 13, the results for different MAFIA models are compared. The results of the homogeneous model are the same as discussed before. The conductivity was again chosen to be 0.88 mho/m and the frequency 900 MHz. The effect of the optical fiber inside the probe can be neglected.

For the more complex model with an optical fiber, ceramic sheets and air holes, γ is about 6% lower than for the homogeneous model. Additional simulations which neglected the ceramic sheets or the air holes revealed that the air holes are responsible for the drop in the conversion factor.

In Figure 14, the frequency dependence of γ is shown for the homogeneous models of MMP and MAFIA and the more complex MAFIA model.

The homogeneous models simulated with MMP and MAFIA are in close agreement with each other. Again, the values for the more complex modeling are slightly lower than those for the homogeneous modeling. In contrast to these findings, the experimentally determined conversion factors are larger than those of the simulations. The reason lies in the fact that even the most complex modeling involves many simplifications of the structure of the real probe. In addition, the electrical parameters of the probe material were not measured, but were taken from the literature. The most important effect is most likely to be the change of the dipole capacitance, which depends on the surrounding media and could not be considered in the simulations. This effect is expected to be more significant for probe designs in which the dipoles are positioned closer to

the surrounding medium.

VII. Conclusions

A procedure has been presented that allows an absolute calibration of the probes for dosimetric assessments with an accuracy of better than ±10%. The chosen approach has the advantage that the calibration setup closely corresponds to that of the actual dosimetric assessments performed with the scanner described in [5]. Thus, further considerations with regard to polarization are not required. If such studies are needed, the techniques described in [5] can be used. Numerical techniques have proven to be adequate to assess the conversion factor γ if a precision of only ±20% is sufficient for this probe. For other probe designs, the uncertainties of the numerically determined conversion factors might be considerably larger.

VIII. Acknowledgments

We gratefully acknowledge the help of Mr. Oliver Egger, Ms. Katja Poković and Mr. Jeroen de Keijzer for their support in this study.

References

[1] H. I. Bassen and G. S. Smith, "Electric field probes – a review," *IEEE Transactions on Antennas and Propagation*, vol. 31, pp. 710–718, Sept. 1983.

[2] T. Schmid and N. Kuster, "Novel E-field probes for close near field scanning," *IEEE Transactions on Vehicular Technology*. submitted.

[3] D. Hill, "Waveguide technique for the calibration of miniature implantable electric-field probes for use in microwave-bioeffects studies," *IEEE Transactions on Microwave Theory and Techniques*, vol. 30, pp. 92–99, Jan. 1982.

[4] N. Kuster and Q. Balzano, "Energy absorption mechanism by biological bodies in the near field of dipole antennas above 300 MHz," *IEEE Transactions on Vehicular Technology*, vol. 41, pp. 17–23, Feb. 1992.

[5] T. Schmid, O. Egger, and N. Kuster, "Automated E-field scanning system for dosimetric assessments," *IEEE Transactions on Microwave Theory and Techniques*, vol. 43, Jan. 1996. in press.

[6] G. Hartsgrove, A. Kraszewski, and A. Surowiec, "Simulated biological materials for electromagnetic radiation absorption studies," *Bioelectromagnetics*, vol. 8, pp. 29–36, Jan. 1987.

[7] C. Gabriel , Personal Communication.

[8] F. Gucker and F. Ayres, "The specific heats of aqueous sucrose solutions," *American Journal of Chemistry*, vol. 59, pp. 447–452, Mar. 1937.

[9] M. Burkhardt, K. Poković, M. Gnos, T. Schmid, and N. Kuster, "Numerical and experimental dosimetry of petri dish exposure setups," *Bioelectromagnetics*, 1996. submitted.

[10] R. R. Bowman, "A probe for measuring temperature in radio-frequency-heated material," *IEEE Transactions on Microwave Theory and Techniques*, vol. 24, no. 1, pp. 43–45, 1976.

[11] Ch. Hafner and L. H. Bomholt, *The 3D Electrodynamic Wave Simulator*. New York: John Wiley & Sons Inc., 1993.

[12] N. Kuster, "Multiple multipole method for simulating EM problems involving biological bodies," *IEEE Transactions on Biomedical Engineering*, vol. 40, pp. 611–620, July 1993.

[13] T. Weiland, "Maxwell's grid equations," *Frequenz 44*, no. 1, 1990.

[14] CST GmbH, Lautenschlaegerstr. 38, D 64289 Darmstadt, *The MAFIA collaboration, User's Guide Mafia Version 3.x.*